Geomechanics and Engineering, *Vol. 38, No. 2 (2024) 125-137*
https://doi.org/10.12989/gae.2024.38.2.125

Effects of chloride ion transport characteristics and water pressure on mechanical properties of cemented coal gangue–fly ash backfill

Dawei Yin*[1], Zhibin Lu[1], Zongxu Li[1], Chun Wang[2], Xuelong Li[1] and Hao Hu**[3]

[1]*State Key Laboratory of Mine Disaster Prevention and Control, Shandong University of Science and Technology, Qingdao 266590, China*
[2]*Henan Polytechnic University, JiaoZuo 454000, China*
[3]*State Key Laboratory of Mining Response and Disaster Prevention and Control in Deep Coal Mines, Anhui University of Science and Technology, Huainan 232001, China*

(*Received March 28, 2024, Revised July 1, 2024, Accepted July 4, 2024*)

Abstract. In paste backfill mining, cemented coal gangue–fly ash backfill (CGFB) can effectively utilize coal-based solid waste, such as gangue, to control surface subsidence. However, given the pressurized water accumulation environment in goafs, CGFB is subject to coupling effects from water pressure and chloride ions. Therefore, studying the influence of pressurized water on the chlorine salt erosion of CGFB to ensure green mining safety is important. In this study, CGFB samples were soaked in a chloride salt solution at different pressures (0, 0.5, 1.5, and 3.0 MPa) to investigate the chloride ion transport characteristics, hydration products, micromorphology, pore characteristics, and mechanical properties of CGFB. Water pressure was found to promote chloride ion transfer to the CGFB interior and the material hydration reaction; enhance the internal CGFB pore structure, penetration depth, and chloride ion content; and fill the pores between the material to reduce its porosity. Furthermore, the CGFB peak uniaxial compression strain gradually decreased with increasing soaking pressure, whereas the uniaxial compressive strength first increased and then decreased. The resulting effects on the stability of the CGFB solid-phase hydration products can change the overall CGFB mechanical properties. These findings are significant for further improving the adaptability of CGFB for coal mine engineering.

Keywords: chloride ion transport; coal gangue–fly ash backfill; fracture morphology; pore analysis; water pressure

1. Introduction

As a major energy source for China, coal is of considerable significance for economic development and social stability (Wang and Song, 2021a, Jie *et al.* 2021, Gao *et al.* 2021). However, the accumulation of coal gangue, fly ash, and other coal-based solid waste generated by coal mining, processing, and combustion not only occupies land resources (Fig. 1(a)) but also exacerbates ecological problems such as soil erosion, geologic desertification, air pollution, and groundwater contamination (Gao *et al.* 2021, Liu and Cheng 2019, Wang *et al.* 2016, Qureshi *et al.* 2020, Hakimi *et al.* 2020). Furthermore, surface subsidence caused by coal mining detrimentally affects the safety of surface structures and the surrounding ecological environment (Fig. 1(b)) (Chen *et al.* 2019, Sun *et al.* 2022, Ma *et al.* 2021). In paste backfill mining, solid waste such as gangue and fly ash is processed into slurry filling materials, which are then pressurized through specialized filling pumps and transported to the gob using filling pipes (Behera *et al.* 2021, Wang *et al.* 2021b). After consolidation and hardening, these dcemented coal gangue–fly ash backfill (CGFB) materials can effectively slow down surface subsidence (Fig. 2(a)) (Li *et al.* 2022a). This process, which consumes coal-based solid waste, thereby relieving pressure on the ecological environment, is widely used in the "green mining" of coal (Li *et al.* 2022a, Helinski *et al.* 2011). In practice, after injection into the gob, CGFB may be soaked in mine water, which is typically rich in chloride ions (Chen *et al.* 2019, Gavrishin, 2018). Chloride ions are thus transported into the CGFB material by osmosis, affecting its performance (Fig. 2(b)). Additionally, the CGFB material becomes hydrated with water containing ions, affecting its stability. Therefore, understanding the CGFB transport characteristics of chloride ions after soaking and the effect of ions on CGFB material properties is critical to maintaining their stable mechanical properties and ensuring green mining safety.

(a) Gangue mountain (b) Surface cracking

Fig. 1 Environmental damage caused by coal mining

*Corresponding author, Professor
E-mail: yindawei@sdust.edu.cn
**Corresponding author, Professor
E-mail: 15056360558@163.com

ISSN: 2005-307X (Print), 2092-6219 (Online)

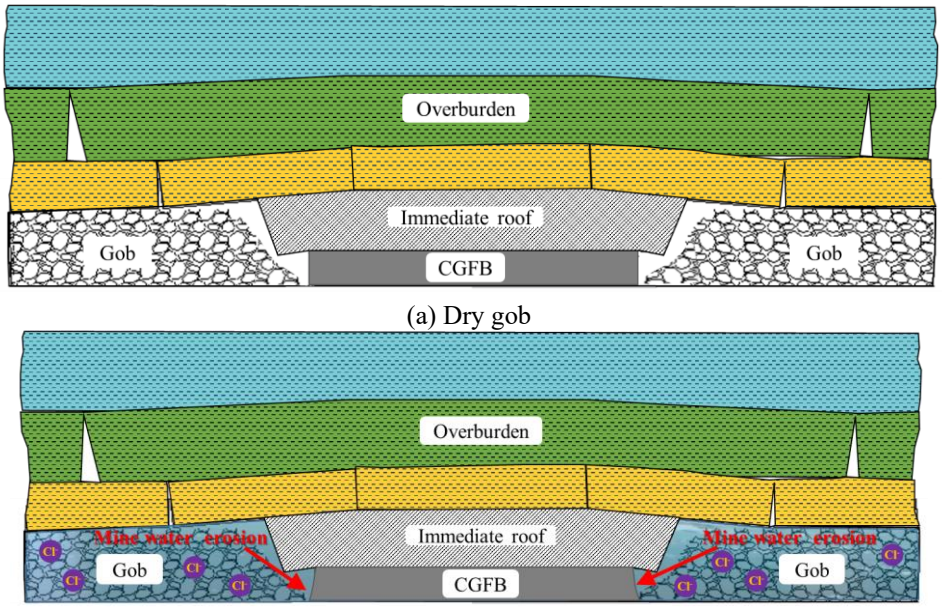

(a) Dry gob

(b) Water-soaked gob

Fig. 2 Process by which CGFB is exposed to mine water. CGFB, cemented coal gangue–fly ash backfill (Li *et al*. 2022).

In terms of ionic attacks, Jiang *et al.* (2022) examined the influence of a chloride salt on the chloride ion diffusion performance of alkali-activated slag mortar and analyzed the chloride ion transmission characteristics of alkali-activated slag mortar. Ngo *et al.* (2023) examined the effects of different cations on the deterioration of paste filling materials. The weakening effect of cations on the filling materials decreased in the following order: Na^+ > Ca^{2+} > Mg^{2+}. Kasap *et al.* (2022) explored the effects of pH on the physicochemical properties and microstructures of paste filling materials. Chen *et al.* (2020) investigated the effects of chloride ions on the mechanical properties of paste filling materials and found that chloride ions initially increased the strength of the samples; however, an accelerated deterioration of the material occurred during the later stages of the test. Xu *et al.* (2022) obtained similar results for paste-filled materials after soaking in chloride and sulfate environments. Further, scanning electron microscopy (SEM) and X-ray diffraction (XRD) observations of the samples were used to elucidate the corrosion mechanism of paste filling materials in chloride and sulfate environments. Orejarena and Fall (2010) predicted the effect of sulfate erosion on the mechanical properties of paste fillings using a neural network, and the obtained predictions correlated well with the experimental results of Xu *et al.* (2022).

These studies have provided important findings on the impact of chloride ionic attacks on the properties of paste filling materials, which can help enhance the effectiveness of filling and mining. However, water in goafs usually exists in a pressurized form (Niu *et al.* 2022), and the effect of mine water pressure on the mechanical characteristics of paste filling materials has not been investigated. In addition, studies on ion erosion have mostly focused on the effects of different ions on the overall strength of paste filling materials rather than on the transport mechanism of ions within these materials. Therefore, in this study, the chloride ion infiltration and diffusion behavior of CGFB under different water pressures (0, 0.5, 1.5, and 3.0 MPa) and the mechanical properties of these samples were investigated. This study aims to provide a theoretical support for accurately evaluating the mechanical properties of paste fillers in backfill mining, thereby increasing mining safety.

2. Materials and methods

2.1 Materials and sample preparation

CGFB samples were prepared from gangue, fly ash, P.042.5 silicate cement and water. Gangue, obtained from the solid waste generated by the Liangjia Coal Mine (Longkou Coal and Electricity Co., Ltd.), was crushed and screened to obtain particles with sizes ≤10 mm. Fly ash was obtained from the Huangdao Power Plant (Qingdao City, Shandong Province) (Li *et al.* 2022). Cement was obtained from the Shandong Rizhao Third Cement Factory (Li *et al.* 2022). The chemical compositions of the raw materials used in the preparation of CGFB are shown in Fig. 3. Water was obtained from a laboratory at the Shandong University of Science and Technology. The soaking solution was prepared using sodium chloride (analytical purity, ≥99% sodium chloride) from Tianjin Hengxing Chemical Reagent Co., Ltd.

CGFB samples with a mass fraction of 78% were prepared using a cement, fly ash, and gangue mass ratio of 1:2:4. The materials were placed in a cement paste mixer and stirred for 8 min. Then, the stirred paste was poured into a 70.7 × 70.7 × 70.7 mm^3 cubic mold, one-third at a time through a vibrating screen to prevent air bubble retention in the sample. After 24 h, the CGFB sample was removed from the mold and placed in a curing box at 20°C

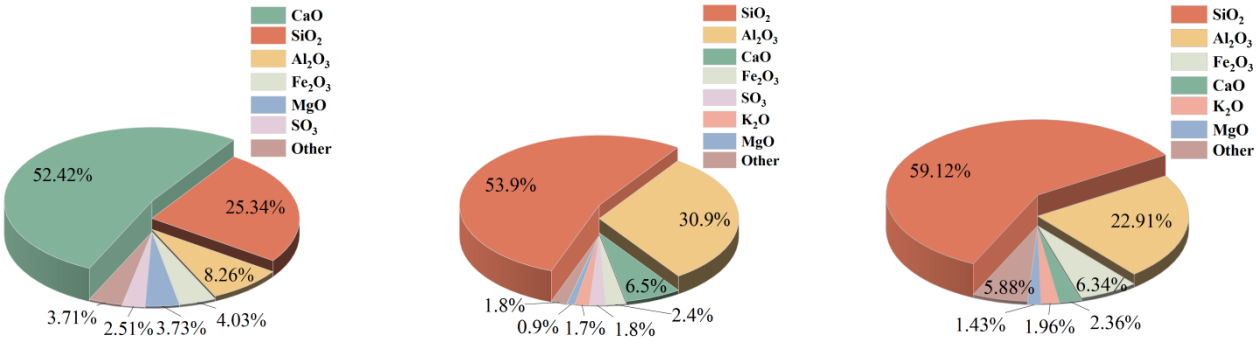

(a) Cement (b) Fly ash (c) Coal gangue

Fig. 3 Chemical compositions of the raw materials used in this study

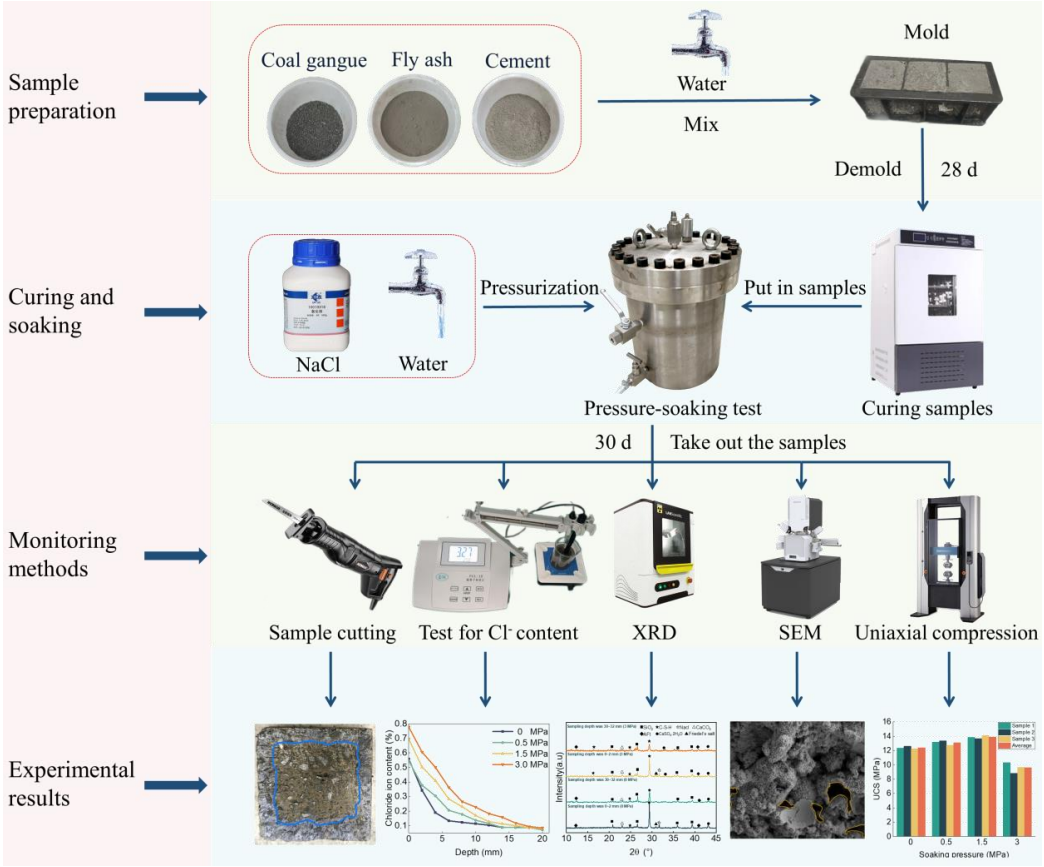

Fig. 4 Overview of the sample preparation and testing procedures. SEM, scanning electron microscopy; XRD, X-ray diffraction

and 95% relative humidity for 28 d. Twenty CGFB samples of the paste-filled body were prepared and divided into four groups (A, B, C, and D) of five samples (labeled A1–A5, B1–B5, C1–C5, and D1–D5). For samples A1, B1, C1, and D1, which were subjected to chloride ion penetration using the salt ponding test and NTBuild 443-94 methods, one side of the surface was selected as the chloride ion erosion surface. The remaining five surfaces were coated with an epoxy resin to ensure that the chloride ions penetrated as far as possible in one dimension. After the epoxy resin was cured, these samples were soaked together with other samples, as described in Subsection 2.2.1. A2, B2, C2, and D2 were used for the chloride ion transport depth test, and A3–5, B3–5, C3–5, and D3–5 were used for the uniaxial compression test.

An overview of the sample preparation procedure and analysis methods used in this study is shown in Fig. 4.

2.2 Monitoring methods

2.2.1 Pressurized soaking

A self-developed pressure soaking device was used in this study (Fig. 5). The device comprised a high-pressure soaking chamber, servo-booster cylinder, pressure sensor,

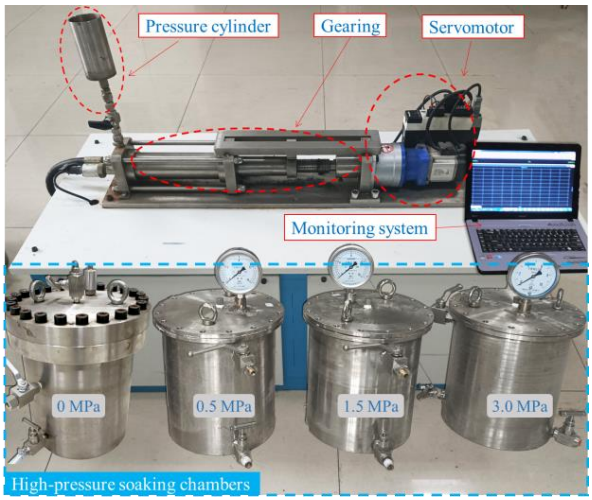

Fig. 5 Overview of the pressure soaking device Yin *et al.* 2022a)

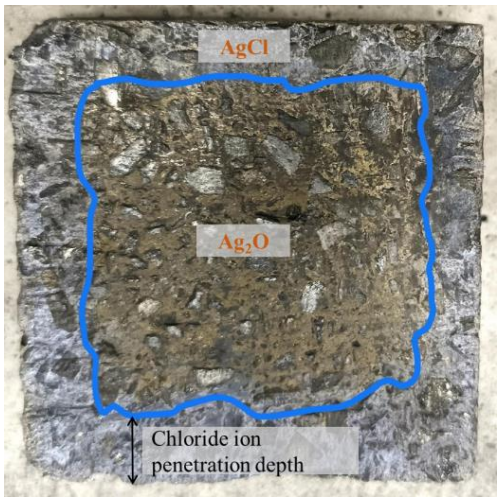

(a) Color changes induced by reaction with silver nitrate

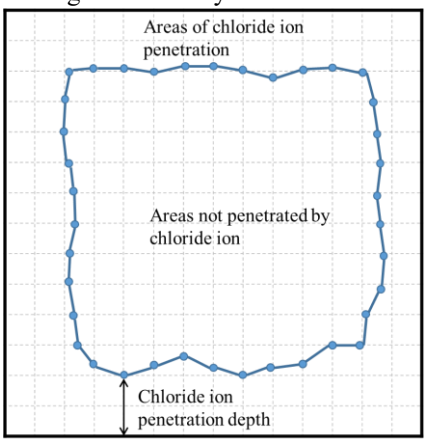

(b) Chloride transport boundary

Fig. 6 Detection of chloride ion penetration depth

digital servo controller, and acquisition system. The stainless-steel high-pressure soaking chamber was cylindrical with inner and outer diameters of 250 and 300 mm, respectively. The top of the chamber was sealed with a rubber ring reinforced with an upper pressure plate to prevent the leakage of pressurized water. The digital servo controller comprised a servomotor connected to a drive booster and digital controller. When filling and pressurizing the soaking chamber, the commands were edited using the operating software on the host computer, sent to the digital servo controller, and transmitted to the servomotor. Through gearing, the servomotor pushed a piston into the booster cylinder to fill and pressurize the soaking chamber. The pressure sensor was connected to the acquisition system for real-time monitoring. Upon achieving the target water pressure, a feedback termination command was sent to the digital controller, and the servomotor stabilized and maintained the pressure, thereby achieving closed-loop control. The soaking solution was 10% NaCl in water, and the immersion duration was 30 d. For groups A–D, the water pressures were 0, 0.5, 1.5, and 3.0 MPa, respectively.

2.2.2 Determination of chloride ion penetration depth

The determination of chloride ion penetration depth was measured by the methods of GB/T15453-2018 After soaking for the required time, the CGFB samples were removed from the soaking solution and the sample surfaces were air dried. Samples A2, B2, C2, and D2 were split in half. The water-soaked leading edge were distinguished from the fracture surface based on color differences. The sample surfaces were sprayed with 1.5 ± 0.3 mL of 0.1 mol/L silver nitrate solution, and photographs were taken after the color was developed. Spraying with silver nitrate solution revealed the demarcation between the white and tan areas. The white and tan areas indicated the chloride ion penetration and impermeable areas, respectively. The chemical reactions involved in the color development process are as follows

$$Ag^+ + Cl^- \rightarrow AgCl \text{ (white)}, \quad (1)$$

$$Ag^+ + OH^- \rightarrow AgOH \rightarrow Ag_2O \text{ (tan)}. \quad (2)$$

Fig. 6(a) shows the color of a CGFB sample after spraying the silver nitrate solution, where the line represents the edge of chloride ion penetration. Using the edge of the penetration, the chloride ion penetration depth was measured for points at 5 mm spacings (Fig. 6(b)). For each sample, the average chloride ion penetration depth d_x was calculated using the following formula

$$d_x = \frac{1}{n}\sum_{i=1}^{n} d_i, \quad (3)$$

where x is the soaking group (A, B, C, or D) and n is the number of measurement points for each CGFB sample.

2.2.3 Determination of chloride ion content

Samples A1, B1, C1, and D1 were ground into layers using a grinder. Based on the chloride ion penetration depth results, the maximum grinding depth was set to 30 mm and 10 layers of powder were removed from each sample. Each powder sample was passed through a 60-mesh sieve and then dried in a 105 °C drying oven until constant weight. After cooling to 20 °C in a desiccator, 2 g of powder from each group was added to a beaker containing 100 mL of

Fig. 7 Filtration and Cl- concentration testing

deionized water. The solution was stirred magnetically for 2 h, and then allowed to stand for 24 h. Subsequently, the upper clear layer was filtered using two layers of filter paper. The chloride ion content of the obtained solution was measured using a chloride ion meter (PCL-1, Hengmag Technology Co.) (Fig. 7).

The measurement was based the formation of an insoluble precipitate (silver chloride) by chloride and silver ions under certain conditions, which induced a change in the electrode potential. When the chloride ion content increased, precipitation increased and the electrode potential changed; thus, the chloride ion content in a water sample can be determined by measuring the potential change. Chloride ion contents of 35.5 g/L to 35.5 μg/L were measured with a resolution of 0.01 pCL and a basic instrument error of ±0.05 pCL.

2.2.4 CGFB sample component detection

A Rigaku Utima IV X-ray diffractometer was used to analyze the phase of the CGFB samples. The device was operated at a voltage of 40 kV and an emission current of 40 mA. The CGFB samples were selected after immersion in a chloride salt solution at pressures of 0 and 3.0 MPa, and powder was taken from the surface of the CGFB samples at 0–2 mm and 30–32 mm inward, respectively. The dried samples were ground through a mortar and sieved through a 200-mesh sieve. After laying the prepared powder sample flat in the groove of the glass carrier sheet, it was placed in the instrument for testing. The test was performed by continuous scanning from 5 to 45° with 0.02° data point intervals and a scanning speed of 4°/min.

2.2.5 Microtopography observations

SEM measurements were performed using an Apreo high-resolution scanning electron microscope with a resolution of 0.8 (15 kV) to 0.9 nm (500 V) and standard magnification of 100–500,000×. The SEM samples had diameters of approximately 15 mm and thicknesses of 10–15 mm. The samples were placed in anhydrous ethanol for 48 h to terminate hydration and then dried in a 55 °C drying oven until constant weight. Because the paste filling material exhibits poor conductivity, the samples were sprayed with gold prior to analysis.

2.2.6 Pore analysis

To quantitatively analyze the fine-scale pore changes in the CGFB samples following soaking under pressure in a chloride salt solution, a particle (pore) and crack analysis system (PCAS) (Yin *et al.* 2021) was used to identify and analyze fracture pores and fissures in the CGFB samples. Using the SEM images of the CGFB samples, the system imported a variety of binarized pore images, automatically removed clutter, segmented and identified pores, output geometric and statistical parameters, displayed the resultant vector images and rose diagrams, and calculated various parameters.

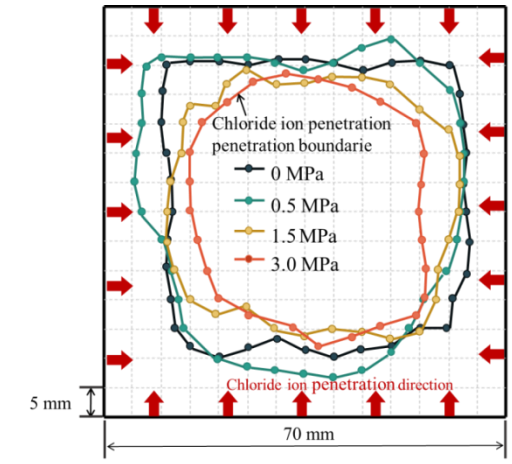

(a) Penetration boundaries at different soaking pressures

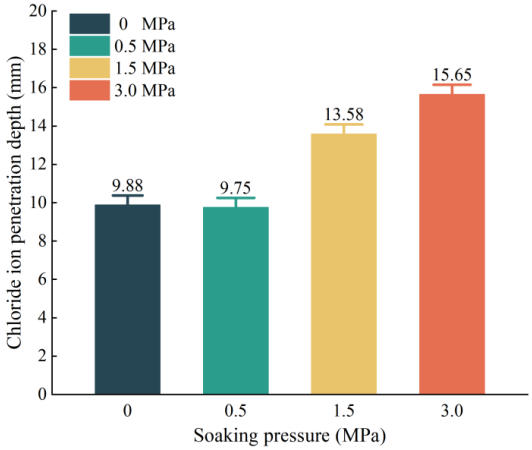

(b) Average penetration depth

Fig. 8 Detection of chloride ion penetration depth

2.2.7 Uniaxial compressive strength (UCS) testing

Uniaxial compression tests were performed using a Shimadzu AG-X250 electronic universal testing machine. The displacement loading was increased at a loading rate of 0.005 mm/s and sample interval of 10 ms until the sample was damaged (Yin *et al.* 2021, Yin *et al.* 2022b, Li *et al.* 2022b, Jiang *et al.* 2023).

3. Results and discussion

3.1 CGFB chloride ion transport characteristics

3.1.1 Chloride ion penetration depth

Fig. 8(a) shows the chloride ion penetration boundary of each sample, and Fig. 8(b) shows the average penetration

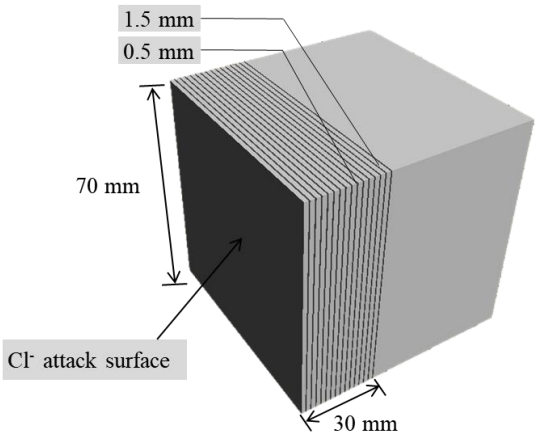

Fig. 9 Sample stratification scheme

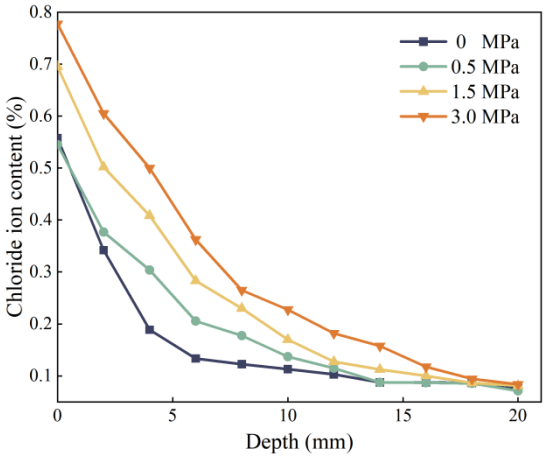

Fig. 10 Dependence of chloride ion content on depth

depth of the CGFB samples under different chloride salt solution pressures. As shown in Fig. 8(b), the soaking pressure significantly affects the penetration depth of the chloride ions. Following soaking in a chloride salt solution at 0 MPa, the penetration depth was 9.88 mm. When the soaking pressure increased from 0 to 0.5 MPa, the chloride ion penetration depth decreased by 1.31% to 9.75 mm. Under a soaking pressure of 1.5 MPa, the chloride ion penetration depth was 13.58 mm, which is 37.45 and 39.28% higher than those at 0 and 0.5 MPa, respectively. When the soaking pressure was increased to 3.0 MPa, the chloride ion permeability of the CGFB sample continued to increase, with a penetration depth of 15.65 mm, which is 58.40 and 15.24% higher than those at 0 and 1.5 MPa, respectively.

These observations indicate that low water pressures (0.5 MPa) have little effect on the CGFB chloride ion penetration depth, whereas high water pressures (1.5 or 3.0 MPa) increase the CGFB chloride ion transport depth. When soaked at low water pressures, no new macroscopic cracks were generated in the CGFB, and the chloride ion infiltration and diffusion was mainly affected by changes in the microstructure of the CGFB samples. Under low water pressures, the CGFB porosity decreased as the soaking pressure increased, thereby hindering chloride ion

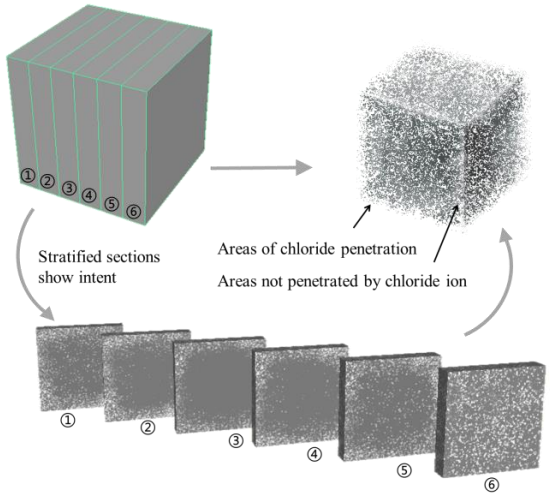

Fig. 11 Distribution of chloride ion in CGFB sample

permeation and diffusion. However, when the soaking pressure exceeded a critical value, new cracks appeared in the CGFB samples and volume expansion occurred. Consequently, the CGFB chloride ion penetration and diffusion capacities increased with increasing water pressure.

An interfacial layer exists between the aggregate and cementitious material in CGFB, which connects the gangue particles and cement fly ash matrix. The interfacial layer cannot effectively transfer stress because it is weaker than the aggregate and paste matrix. Under high-pressure water, the microcracks in the interfacial layer of CGFB expand rapidly, enhancing the chloride ion transportation capacity.

3.1.2 Chloride ion content

The chloride ion contents in different layers of the CGFB samples soaked in chloride salt solutions at 0, 0.5, 1.5, and 3.0 MPa were examined. The layer sampling scheme is shown in Fig. 9, and the chloride ion contents at different pressures and depths are shown in Fig. 10. The distribution of chloride ions in the CGFB sample after soaking in pressurized chloride solution is shown in Fig. 11. If the chloride ion distribution curve was stable over the penetration depth, the determined depth value was consistent with the data in Subsection 3.1.1. As shown in Fig. 10, when the sampling depth increases, the free chloride ion content in the CGFB samples gradually decreases. At a sampling depth of 6 mm, the chloride ion contents of the CGFB samples immersed in chloride salt solution at 0, 0.5, 1.5, and 3.0 MPa were 76.05, 62.29, 59.28, and 53.38% lower than that at the surface, respectively. For the sample soaked at 0 MPa, the chloride ion content decreased more rapidly as the penetration depth increased compared with the samples exposed to higher soaking pressures. At the same sampling depth, the CGFB samples soaked at higher pressures had higher chloride ion contents. When the sampling depth was less than 5 mm, the chloride ion contents of the samples soaked at pressures of 0 and 0.5 MPa were similar but lower than those of the samples soaked at pressures of 1.5 and 3.0 MPa. At

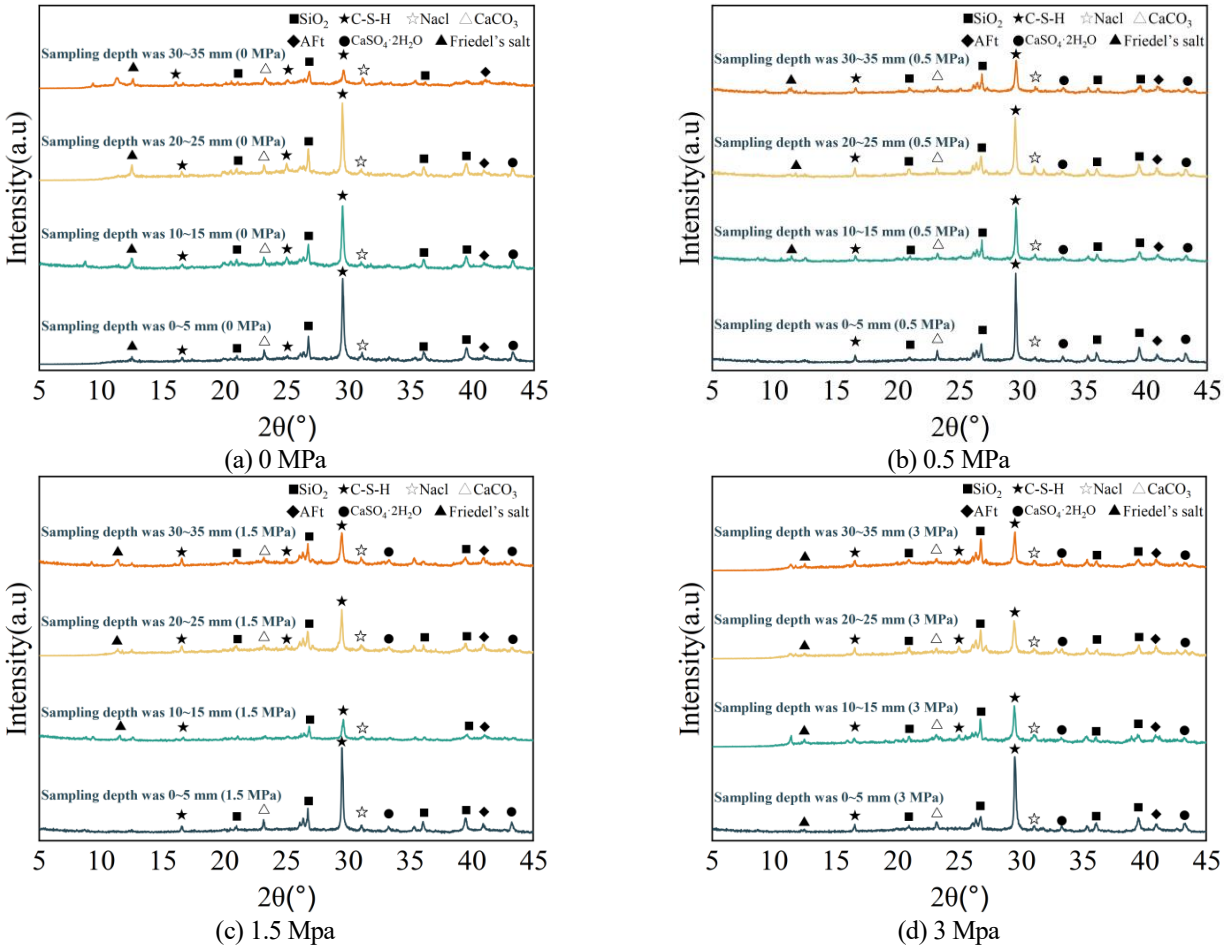

Fig. 12 XRD pattern of CGFB sample

sampling depths of 0–15 mm, the chloride ion contents of each group of samples differed significantly, with a higher soaking pressure resulting in a higher chloride ion content. When the sampling depth was greater than 10 mm, the differences between the chloride ion contents of the samples soaked at 0, 0.5, and 1.5 MPa decreased, but the chloride ion content of the sample soaked at 3.0 MPa remained notably higher. When the sampling depth was greater than 20 mm, the chloride ion contents of all the CGFB samples were similar, regardless of the soaking pressure, to that of the material not subjected to chloride salt soaking.

These results suggest that water pressure promotes the transfer of chloride ions inside CGBF, as the chloride ion gradient within the material becomes less steep and the chloride ion content at each depth increases with increasing water pressure.

At 0 MPa, chloride ions were only transferred into the CGFB through a concentration gradient effect; however, under pressurized water, chloride ions were transported into the CGFB samples via both concentration and pressure gradients, resulting in greater immobilization inside the CGFB samples. As discussed in Subsection 3.1.1, pressurized water changes the internal pore structure of CGFB, which promotes the transportation of chloride ions within this material.

3.1.3 X-ray diffraction analysis

To fully understand the effect of chloride ion transmission on the physical phase composition of filling pastes under water pressure, the CGFB samples were selected under different immersion pressures. The powder was taken from the surface of the sample at a depth of about 0 to 5 mm, and was taken inward every 10 mm , until reached to the sample center(depth of 35mm). the physical phases of the CGFB samples were analyzed using the X-rays of rocks. The XRD pattern of the CGFB samples is shown in Fig. 12.

From Fig. 12, it can be seen that when the sampling depth is 0–5 mm, the main physical phases inside the CGFB samples under chloride salt solution immersion are quartz (SiO_2), gypsum ($CaSO_4{\cdot}2H_2O$), ettringite (AFt), calcite ($CaCO_3$), and C-S-H gel. As the sampling depth increased, the diffraction peak of the hydration product C-S-H in the XRD pattern of the sample significantly decreased, indicating that the penetration of chlorinated brine promotes the hydration reaction of CGFB, which is consistent with the conclusions of previous studies. As the water pressure increased, the diffraction peak of the hydration product first increased, then remained unchanged, and finally decreased. This indicates that under low water pressure, the ability of chlorinated brine to promote hydration reactions of CGFB increases with increased pressure. When the pressure reaches a certain critical range, the ability of the water pressure to promote hydration reactions maintains a

stable rate, and when the pressure exceeds this critical range, the ability of the water pressure to promote hydration reactions gradually decreases.

The diffraction peak of AFt, another hydration product, decreased with increasing water pressure, indicating that chloride ions combine with tricalcium aluminate ($3CaO{\cdot}Al_2O_3$), which is not involved in the hydration reaction, and replace the sulfate of calomel (AFt) to produce Friedel's salt. Friedel's salt diffraction peaks appear in the XRD spectra of the surface powder of the CGFB samples solidly immersed in each pressurized chloride salt solution. Friedel's salt fills in the internal pores of the CGFB sample, changing its pore structure and improving its densification.

3.1.4 Chloride ion transport mechanisms in CGFB

When CGFB is unsaturated, chloride ion transport is affected by capillary adsorption (Sanchez *et al.* (2020). When a CGFB sample is in contact with the chloride salt solution, the difference between the attraction of the internal liquid to the surface molecules and the attraction of the solid to the surface molecules results in an interfacial energy on the solid–liquid surface. Owing to this phenomenon, liquid can be sucked into the pores to a certain depth, forming a curved surface. Capillary adsorption generally occurs in shallow parts of the solid material, and is more rapid than other transport processes (Yedra *et al.* 2022; Pedro *et al.* (2015). Ionic transport within water-saturated CGFB is no longer affected by capillary adsorption, and chloride ions are transported through the CGFB via diffusion, which involves the migration of free molecules or ions from a region of high concentration to one of low concentration driven by a concentration difference (Park *et al.* 2014). When CGFB is saturated with water, a concentration gradient is created between the surface and internal pore solution, and chloride ions diffuse into the CGFB. The diffusion of chloride ions into the CGFB can be described using Fick's second law, as follows

$$C_x = (C_s - C_0)\left[1 - erf\frac{x}{2\sqrt{Dt}}\right] + C_0, \quad (4)$$

where C_x is the chloride ion content (%) at depth x and time t (s), C_s is the chloride ion content on the surface (%), C_0 is the initial chloride ion content (%), and D is the chloride ion migration coefficient of CGFB under water pressure (mm^2/s).

When the CGFB sample soaked at 0 MPa was saturated with water, chloride ions in the interior were transported via pure diffusion. When the outer surface of the CGFB encountered pressurized water, a hydraulic gradient was generated from the outer surface to the interior, resulting in a seepage field. Therefore, chloride ion transport within the CGFB samples soaked at 0.5, 1.5, and 3.0 MPa was also affected by osmosis. Osmosis is the process of chloride ion migration from the solution to the interior of a sample under hydrostatic pressure. Previous studies have found that the osmotic transport of ions within porous materials in high hydrostatic pressure environments follows Darcy's law (Jabeen *et al.* 2019; Aminpour *et al.* 2018; Leng *et al.* 2021)

$$v(t) = \frac{K}{\rho g}\frac{\Delta H}{\Delta x}, \quad (5)$$

where t is the infiltration time (s), $v(t)$ is the seepage velocity (m/s), ΔH is the total head loss (MPa), Δx is the seepage path length, K is the hydraulic conductivity, and ρ is the fluid density (kg/m^3).

For the CGFB samples in the chloride salt solution, the chloride ions initially migrated into the interior via capillary adsorption. Once some of the solution entered the CGFB but the CGFB was not yet saturated, the chloride ions in the sample at 0 MPa migrated inside the CGFB via capillary adsorption and diffusion, whereas the chloride ions in the samples at 0.5, 1.5, and 3.0 MPa were transported to the interior via capillary adsorption, diffusion driven by the concentration gradient, and osmosis driven by the pressure gradient. After completion of the pressurization process, the stress within the CGFB samples reached equilibrium (i.e., there is no pressure difference between the inside and outside of the sample). At this time, ion transport within the samples was mainly affected by capillary adsorption and diffusion. After water saturation, no further capillary adsorption occurred within the samples, and the chloride ion transport only occurred via diffusion.

Under high-pressure water, the microcracks inside the CGFB samples were compacted or slipped, producing a local stress release or stress concentration phenomenon. Simultaneously, chloride ions entered the CGFB, and unreacted raw materials or hydration products generated secondary hydration products or salt corrosion products that filled the internal pores. Secondary hydration products and salt corrosion products continued to form and gradually occupied the surrounding pores, thereby changing the internal pore structure of the CGFB samples. Under the mechanical action of water pressure and the physical and chemical action of chloride salt, local stress adjustment occurred within the CGFB samples, which caused the liquid in the pores to produce a local pressure difference. Therefore, after reaching saturation, the chloride ions inside the CGFB still exhibited osmotic behavior.

The soaking pressure mainly influenced the osmosis and diffusion of chloride ions in CGFB through osmosis driven by the pressure gradient, which promoted the entry of chloride ions into the CGFB, allowing chloride ions to react more completely with the backfill material components. The salt corrosion products crystallized and expanded, and the internal CGFB pore structure changed, which can promote or inhibit the transport of chloride ions. However, under the influence of surface tension and volume compression by water, free water in the cracks can induce splitting and pulling, thereby promoting the development and expansion of primary cracks and the generation of new cracks inside the CGFB. The expansion and increase in microcracks increases the permeability coefficient, which in turn promotes the transportation of chloride ions into the CGFB.

3.2 Micromorphology

Fig. 13 shows cross-sectional SEM images of the CGFB samples soaked in a chloride salt solution at different sampling depths under different pressures (0, 0.5, 1.5, and 3.0 MPa). The CGFB samples soaked at different pressures exhibited similar morphologies. However, at increased water pressures, the CGFB structure gradually became denser and the amount of connecting pores increased. This paste filler, a typical porous

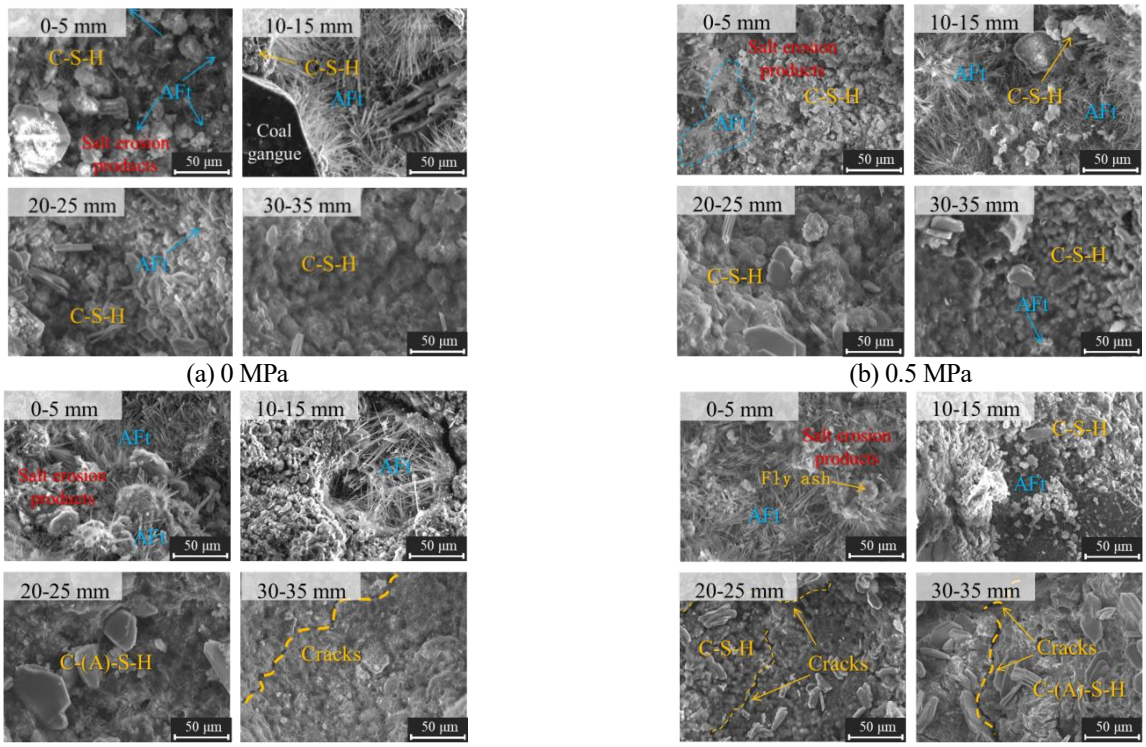

Fig. 13 SEM images of microstructures of CGFB soaked in chloride salt solution at different pressures and different sampling depth

material, and chloride ions, which infiltrate the CGFB, can react with tricalcium aluminate ($3CaO{\cdot}Al_2O_3$; C3A), which is not involved in the CGFB hydration reaction, to produce Friedel's salt (FS). Chloride ions can also displace sulfate from calcium alumina (AFt) to produce FS and Kuzel's salt (KS).

As shown in Fig. 13(a), the CGFB soaked at 0 MPa has a relatively loose structure, with numerous irregularly shaped pores. The hydration products appear as a small number of rods and lumps of calcite bonded to the C-S-H cementation structure. Some clusters of flocculated salt-etching crystallization products are also observed. Under pressurized water, the CGFB had a relatively loose matrix and the hydration products were compacted, partly filling the pores. Simultaneously, the mechanical effect of water promoted the expansion of the primary pores and the development and penetration of larger pores. When the water pressure increased from 0 to 0.5 MPa, the CGFB structure became denser, the number of small pores decreased, and the number of larger connecting pores increased (Fig. 13(b)). As the weakest region of the CGFB material, the interfacial transition zone between the aggregate and paste is susceptible to deterioration under water pressure. When the water pressure increased to 1.5 MPa, more microcracks appeared in the interfacial transition zone (Fig. 13(c)). As shown in Fig. 13(d), the pore area of CGFB continued to increase and the microcracks expanded at 3.0 MPa. Simultaneously, some fly ash shedding can be observed. This phenomenon can be explained by the lubrication and softening effects of water, which can decrease the friction coefficient and cohesion between particles within the CGFB. Poorly cemented materials, such as fly ash, are eroded by high-pressure water.

As seen in Fig. 13, the hydration products observed in the SEM spectrum decrease significantly as the sampling depth increases, and this characteristic becomes more and more obvious as the water pressure decreases. Compared with those in the sample soaked at 0 MPa, the chloride ions in the samples soaked at higher pressures were transported deeper within the CGFB, increasing the chloride ion content at the same penetration depth. Under pressurized water, the loose structure within the CGFB was compacted, which reduced the porosity to a certain extent. With increasing water pressure, the primary pores within the material expanded, and numerous cracks were generated in the interfacial transition zone. The formation and expansion of cracks accelerate solution infiltration, which can promote hydration and salt corrosion of the surrounding CGFB materials. The obtained products partly filled the pores, which impacted the intrusion of chloride ions. Driven by the hydraulic pressure and concentration gradients as well as pore connection and expansion, the chloride ion transport into the CGFB was accelerated. The compaction effect of the high-pressure solution on the loose material and the crystallization and expansion of the hydration and salt erosion products caused the internal pores of CGFB to decrease, preventing the chloride ion inside the CGFB. Owing to the interplay of these factors, the chloride ion penetration depth of the CGFB soaked at 0.5 MPa was similar to that soaked at 0 MPa. With increased water pressure, the influences of the pressure gradient and pore expansion on chloride ion transport became dominant, resulting in a significant increase in the chloride ion penetration depth of the CGFB samples soaked at 1.5 and 3.0 MPa. This behavior is consistent with the chloride ion penetration depth results in Subsection 3.1.1.

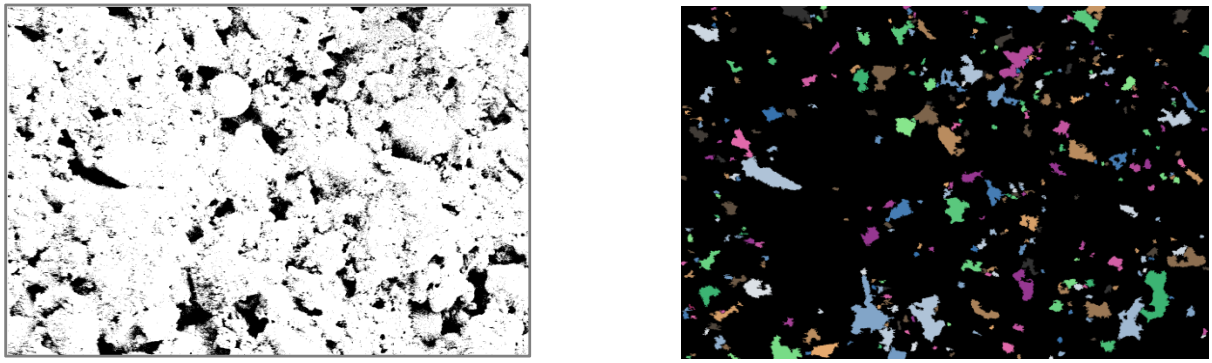

(a) Binary image (b) Rose diagram

Fig. 14 Pore distribution of CGFB soaked in chloride salt solution at 0.5 MPa

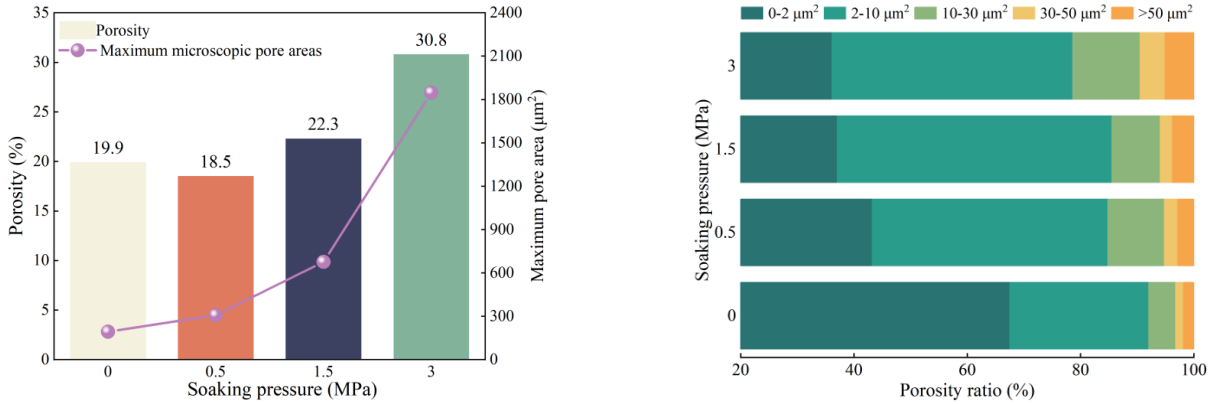

(a) Relationship between porosity, maximum pore area, and solution pressure (b) Pore area distributions

Fig. 15 Pore size characteristics of CGFB samples soaked at different pressures

Fig. 14 shows the pore distribution image of CGFB soaked at 0 MPa, as processed using the PCAS image software. In the binary image in Fig. 14(a), the pore regions appear black and the CGFB material aggregate and matrix appear white. Figure 14(b) shows the rose diagram obtained by further processing of the binary image using the PCAS software; the pore regions are colored, with different colors corresponding to different pore areas, and the nonporous region is black. The pore size characteristics of the CGFB samples soaked at different pressures are shown in Fig. 15. Figure 15(a) shows the relationship between sample porosity, maximum pore area, and solution pressure, and Fig. 15(b) shows the CGFB pore area distributions.

The soaking pressure had a significant effect on the porosity of CGFB (Fig. 15(a)). The porosity of the CGFB samples first decreased and then increased as the soaking pressure increased. When the soaking pressure increased from 0 to 0.5 MPa, the porosity of the CGFB sample decreased by 7.03%. When the soaking pressure increased to 1.5 and 3.0 MPa, the porosities of the CGFB samples were 10.76 and 54.77% higher, respectively, than that of the sample soaked at 0 MPa. Moreover, the maximum microscopic pore areas increased with increasing soaking pressure (193.3, 307.4, 676.7, and 1847.8 μm^2 at 0, 0.5, 1.5, and 3.0 MPa, respectively). Upon entering the CGFB, the pressurized solution compacted the material matrix, hydration products, and salt erosion products, which reduced the porosity. At higher water pressures, the increased load induced splitting and pulling of the internal cracks in the CGFB, resulting in crack expansion and pore penetration, which increased the porosity and maximum pore area.

As shown in Fig. 15(b), at 0 MPa, most pores were smaller than 2 μm^2 (67.21%), with some 2–10 μm^2 pores (24.42%) but relatively few pores with areas of 30–50 μm^2 (1.41%) or greater than 50 μm^2 (1.82%) appeared. At 0.5 MPa, the proportion of pores with an area of less than 2 μm^2 decreased (42.91%), and the proportion of pores with an area of 2–10 μm^2 increased (41.27%). As the soaking pressure increased, the proportion of pores with areas of less than 2 μm^2 gradually decreased, whereas the proportion of larger pores (>50 μm2) increased. At 3.0 MPa, 35.78% of pores were less than 2 μm^2 (46.76% less than that at 0 MPa); however, 5.50% of pores were larger than 50 μm^2 (177.48% more than at 0 MPa). These changes in the pore characteristics are due to the mechanical action of water, hydration and salt etching product crystallization, and CGFB structure expansion, which filled small pores and developed larger pores.

3.3 Mechanical characteristics of CGFB

Figs. 16 and 17 shows the UCS and peak strain of samples under different soaking pressures It can be seen from figure that at lower soaking pressures (<3.0 MPa), the average UCS of the CGFB samples increased with increasing water pressure.

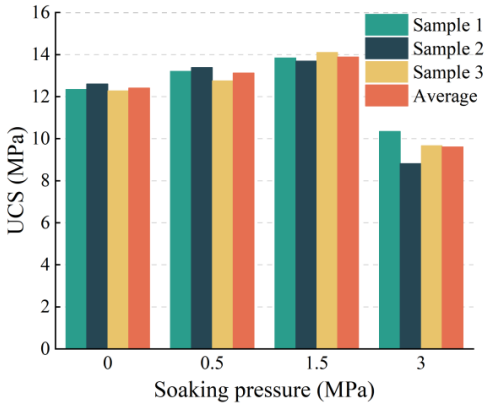

Fig. 16 UCS of the CGFB samples. UCS, uniaxial compressive strength.

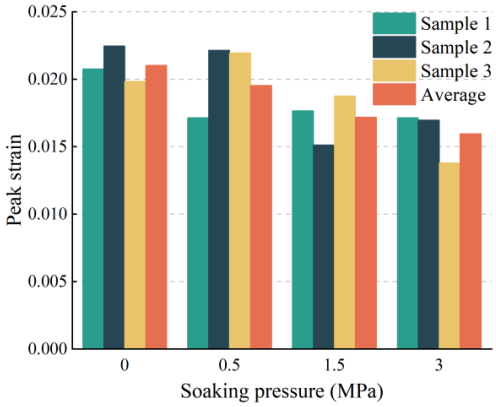

Fig. 17 Peak strain of CGFB samples under uniaxial compression test

The maximum average UCS value of the CGFB samples was 13.88 MPa at 1.5 MPa, which was 11.88% higher than that at 0 MPa. At 3.0 MPa, the average UCS decreased to 9.61 MPa, which was 25.27% lower than that at 1.5 MPa. The average peak strain of the CGFB samples gradually decreased with increasing soaking pressure. The values for the samples soaked at 0.5, 1.5, and 3.0 MPa were 7.04, 18.24, and 30.76% lower than that soaked at 0 MPa, respectively. This phenomenon can be explained by the changes in the CGFB pore structure under external water pressure. At a higher pressure, the loose internal structure was compacted, which increased the strength of the CGFB samples. However, the increased compactness also increased the brittleness of the CGFB samples. Thus, the peak strain decreased as the soaking pressure increased. Simultaneously, the movement of the pressurized solution within the microcracks resulted in a surface load, generating a splitting force and accelerating the expansion of microcracks and pores within the CGFB samples; this deterioration increased the chloride ion permeability. In addition, the pore solution composition changed under water pressure and chloride ion content gradients, which affected the stability of the solid-phase hydration products. As the water pressure increased, the chloride ion penetration depth and content increased and the chloride ions became immobilized within the CGFB through the physicochemical effect. Owing to the resulting leaching, decomposition, and crystallization expansion of the filling material components, the pores were partly filled, increasing the strength of the CGFB samples. When the water pressure was high (>3.0 MPa), the cleavage force of the pressurized solution on the internal cracks played a dominant role and the mechanical properties deteriorated, decreasing the UCS.

4. Conclusions

In this study, CGFB samples were soaked in a chloride salt solution at different pressures (0, 0.5, 1.5, and 3.0 MPa) to investigate chloride ion transport, fine pore characteristics, and strength performance under hydraulic pressure. The main conclusions are as follows.

(1) A low water pressure (0.5 MPa) had little effect on chloride ion penetration into the CGFB, whereas higher water pressures significantly increased the penetration depth. The chloride ion penetration depths of the CGFB samples soaked at 1.5 and 3.0 MPa were 37.45 and 58.40% higher, respectively, than that soaked at 0 MPa.

(2) Pressurized water promoted the transport of chloride ions inside the CGFB samples. The chloride ion gradient within the material became less steep as the water pressure increased. At the same sampling depth, a higher soaking pressure resulted in a higher chloride ion content within the CGFB samples.

(3) Upon increasing the soaking pressure, the proportion of small pores (<2 μm^2) decreased, whereas the proportion of larger pores (>50 μm^2) increased. At the maximum soaking pressure (3.0 MPa), the sample had 46.76% less small pores and 177.48% more larger pores than the sample soaked at 0 MPa.

(4) The peak strain of the CGFB samples gradually decreased as the soaking pressure increased, whereas the UCS increased to a maximum and then decreased. Owing to effects of water pressure on the internal pore structure of CGFB as well as the penetration depth and content of chloride ions, the stability of the solid-phase hydration products inside the CGFB changed, which influenced the overall mechanical properties of the CGFB samples.

(5) At the present stage, only analysis of the hydration reaction with chloride ion on four different water pressurehas been conducted. In future research, will analysis of the hydration reaction with chloride ion and filling materials on different water pressurehas.

These findings are significant for further improving the adaptability of CGFB for coal mine engineering. The transport of chloride ions under hydraulic pressure is a complicated process, and Fick's second law and Darcy's law, which have been commonly used in previous studies, cannot accurately describe this process. Thus, further studies should be conducted to model chloride ion transportation into CGFB under hydraulic pressure. Improving the performance of the filler material is critical for the long-term safety and stability of backfilled mines.

Acknowledgments

The research described in this paper was financially

supported by the National Natural Science Foundation of China [Grant Nos. 52274128 and 52174159], the Taishan Scholars Project Special Fund, the Open Fund for the Henan Key Laboratory for Green and Efficient Mining & Comprehensive Utilization of Mineral Resources (KCF2204), and the Open Fund for the State Key Laboratory of Mining Response and Disaster Prevention and Control in Deep Coal Mines [Grant No. SKLMRDPC22KF01].

We would like to thank Editage (www.editage.cn) for English language editing.

References

Aminpour, M., Galindo-Torres, S.A., Scheuermann, A. and Li, L. (2018), "Pore-scale behavior of darcy flow in static and dynamic porous media", *Phys. Rev. Appl.*, **9**, 064025. https://doi.org/10.1103/PhysRevApplied.9.064025.

Behera, S.K., Mishra, D.P., Singh, P., Mishra, K., Mandal, S.K., Ghosh, C.N., Kumar, R. and Mandal, P.K. (2021), "Utilization of mill tailings, fly ash and slag as mine paste backfill material: Review and future perspective", *Constr. Build. Mate*r., **309**, 125120. https://doi.org/10.1016/j.conbuildmat.2021.125120.

Chen, S.J., Yin, D.W., Cao, F.W., Liu, Y. and Ren, K.Q. (2016), "An overview of integrated surface subsidence-reducing technology in mining areas of China", *Nat. Hazards.*, **81**, 1129-1145. https://doi.org/10.1007/s11069-015-2123-x.

Chen, Y., Zhu, S. and Xiao, S. (2019), "Discussion on controlling factors of hydrogeochemistry and hydraulic connections of groundwater in different mining districts", *Nat. Hazards.*, **99**, 689-704. https://doi.org/10.1007/s11069-019-03767-1.

Chen, S.J., Du, Z.W., Zhang, Z., Zhang, H.W., Xia, Z.G. and Feng, F. (2020), "Effects of chloride on the early mechanical properties and microstructure of gangue-cemented paste backfill", *J. Environ. Manag.*, **23**, 117504. https://doi.org/10.1016/j.conbuildmat.2019.117504.

Gao, H.D., Huang, Y.L., Li, W., Li, J.M., Ouyang, S.Y., Song, T., Lv, F., Zhai, W. and Ma, K. (2021), "Explanation of heavy metal pollution in coal mines of China from the perspective of coal gangue geochemical characteristics", *Environ. Sci. Pollut. Res. Int.*, **28**, 65363-65373. https://doi.org/10.1007/s11356-021-14766-w.

Gavrishin, A.I. (2018), "Formation patterns of the chemical composition of mine waters in eastern Donbas", *Dokl. Earth Sci.*, **481**, 916-917. https://doi.org/10.1134/S1028334X18070127.

Hakimi, M., Kiani, P., Alikhani, M., Feizi, N., Bajestani, A.M. and Alimard, P. (2020), "Reducing environmental pollution of fuel fly ash by extraction and removal vanadium pentoxide", *Solid Fuel Chem.*, **54**, 337-342. https://doi.org/10.3103/S0361521920050055.

Helinski, M., Fahey, M. and Fourie, A. (2011), "Behavior of cemented paste backfill in two mine stopes: Measurements and modeling", *J. Geotech. Geoenviron. Eng.*, **137**, 171-182. https://doi.org/10.1061/(ASCE)GT.1943-5606.0000418.

Jabeen, I., Farooq, M. and Mir, N.A. (2019), "Variable mass and thermal properties in three-dimensional viscous flow: Application of Darcy law", *J. Cent. South Univ.*, **26**, 1271-1282. https://doi.org/10.1007/s11771-019-4086-7.

Jiang, L.H., Niu, Y.L., Jin, W.Z., Gao, H.L. and Chen, L. (2022), "Influence of chloride salt type on chloride ion diffusion performance of alkali-activated slag mortar", *Constr. Build. Mater.*, **351**, 128930. https://doi.org/10.1016/j.conbuildmat.2022.128930.

Jiang, N., Lv, K., Gao, Z., Jia, C., Ye, L., Meng, S. and Su, Q. (2023), "Experimental study on mechanical properties of single fracture-hole red sandstone", *Front. Earth Sci.*, **10**, 1083689. https://doi.org/10.3389/feart.2022.1083689.

Jie, D.F., Xu, X. and Guo, F. (2021), "The future of coal supply in China based on non-fossil energy development and carbon price strategies", *Energy*, **220**, 119644. https://doi.org/10.1016/j.energy.2020.119644.

Kasap, T., Yilmaz, E. and Sari, M. (2022), "Physico-chemical and micro-structural behavior of cemented mine backfill: Effect of pH in dam tailings", *J. Environ. Manage.*, **314**, 115034. https://doi.org/10.1016/j.jenvman.2022.115034.

Leng, J.Y., Lin, X.B. and Wang, L.L. (2021), "Effects of osmosis on darcy flow in shales", *Energy Fuels.*, **35**, 4874–4884. https://doi.org/10.1021/acs.energyfuels.0c03924.

Liu, X. and Cheng, Z. (2019), "Changes in subsidence-field surface movement in shallow-seam coal mining", *J. S. Afr. Inst. Min. Metall.*, **119**, 201-206. https://doi.org/10.17159/2411-9717/2019/v119n2a12.

Li, Z.X., Yin, D.W., Jiang, N., Wang, F., Ding, Y.S. and Li, F.X. (2022a), "Deformation and failure characteristics of bimaterial samples consisting of sandstone and cemented coal gangue–fly ash backfill under uniaxial loading", *Mineral.*, **12**, 2. https://doi.org/10.3390/min12121546.

Li, F.X., Yin, D.W., Wang, F., Jiang, N. and Li, X.L. (2022b), "Effects of combination mode on mechanical properties of bi-material samples consisting of rock and coal", *J. Mater. Res. Technol.*, **19**, 2156-2170. https://doi.org/10.1016/j.jmrt.2022.05.174.

Ma, J.B., Yin, D.W., Jiang, N., Wang, S. and Yao, D.H. (2021), "Application of a superposition model to evaluate surface asymmetric settlement in a mining area with thick bedrock and thin loose layer", *J. Cleaner Product.*, **314**, 128075. https://doi.org/10.1016/j.jclepro.2021.128075.

Ngo, I., Ma, L.Q., Zhai, J.T., Wang, Y.Y. and Wei, T.X. (2023), "Durability of CO2-fly ash-based backfill materials in cation water deterioration", *Int. J. Min. Reclam. Environ.*, **37**, 544-567. https://doi.org/10.1080/17480930.2023.2216498.

Niu, X.H., Feng, G.R., Liu, Q., Han, Y.N. and Qian, R.P. (2022), "Numerical investigation on mechanism and fluid flow behavior of goaf water inrush: A case study of Dongyu coal mine", *Nat. Hazards.*, **113**, 1783-1802. https://doi.org/10.1007/s11069-022-05369-w.

Orejarena, L. and Fall, M. (2010), "The use of artificial neural networks to predict the effect of sulphate attack on the strength of cemented paste backfill", *Bull. Eng. Geol. Environ.*, **69**, 659-670. https://doi.org/10.1007/s10064-010-0326-7.

Park, B., Jang, S.Y., Cho, J.Y. and Kim, J.Y. (2014), "A novel short-term immersion test to determine the chloride ion diffusion coefficient of cementitious materials", *Constr. Build. Mater.*, **57**, 169-178. https://doi.org/10.1016/j.conbuildmat.2014.01.086.

Pedro, D., de Brito, J. and Evangelista, L. (2015), "Performance of concrete made with aggregates recycled from precasting industry waste: influence of the crushing process", *Mater. Struct.*, **48**, 3965-3978. https://doi.org/10.1617/s11527-014-0456-7.

Qureshi, A.A., Kazi, T.G., Baig, J.A., Arain, M.B. and Afridi, H.I. (2020), "Exposure of heavy metals in coal gangue soil, in and outside the mining area using BCR conventional and vortex assisted and single step extraction methods. Impact on orchard grass", *Chemosphere*, **255**, 126960. https://doi.org/10.1016/j.chemosphere.2020.126960.

Sanchez, T., Conciatori, D., Laferriere, F. and Sorelli, L. (2020), "Modelling capillary effects on the reactive transport of chloride ions in cementitious materials", *Cement. Concrete Res.*, **131**, 106033. https://doi.org/10.1016/j.cemconres.2020.106033.

Sun, Q., Wei, X.D. and Wen, Z.J. (2022), "Preparation and strength formation mechanism of surface paste disposal materials in coal mine collapse pits", *J. Mater. Res. Technol.*, **17**, 1221-1231. https://doi.org/10.1016/j.jmrt.2022.01.062.

Wang, S., Luo, K., Wang, X. and Sun, Y.Z. (2016), "Estimate of sulfur, arsenic, mercury, fluorine emissions due to spontaneous combustion of coal gangue: An important part of Chinese emission inventories", *Environ. Pollut.*, **209**, 107-113. https://doi.org/10.1016/j.envpol.2015.11.026.

Wang, Q. and Song, X.X. (2021a), "Why do China and India burn 60% of the world's coal? A decomposition analysis from a global perspective", *Energy*, **227**, 120389. https://doi.org/10.1016/j.energy.2021.120389.

Wang, J., Zhang, C., Fu, J.X., Song, W.D. and Zhang, Y.F. (2021b), "Effect of water saturation on mechanical characteristics and damage behavior of cemented paste backfill", *J. Mater. Res. Technol.*, **15**, 6624-6639. https://doi.org/10.1016/j.jmrt.2021.11.078.

Xu, G., Fan, K., Wang, K. and Ning, J. (2022), "Paste backfill corrosion mechanisms in chloride and sulfate environments", *Minerals*., **12**, 551. https://doi.org/10.3390/min12050551.

Yedra, E., Ferrández, D., Morón, C. and Saiz, P. (2022), "New test methods to determine water absorption by capillarity. Experimental study in masonry mortars", *Constr. Build. Mater.*, **319**, 125988. https://doi.org/10.1016/j.conbuildmat.2021.125988.

Yin, D.W., Ding, Y.S., Jiang, N., Li, F.X., Zhang, J.C. and Xu, H.H. (2022a), "Mechanical properties and damage characteristics of coal samples under water immersion pressure", *Lithosphere*., **10**, 1278783. https://doi.org/10.2113/2022/1278783.

Yin, D.W., Chen, S.J., Ge, Y. and Liu, R. (2021), "Mechanical properties of rock-coal bi-material samples with different lithologies under uniaxial loading", *J. Mater. Res. Technol.*, **10**, 322–338. https://doi.org/10.1016/j.jmrt.2020.12.010.

Yin, D.W., Chen, S.J., Sun, X.Z. and Jiang, N. (2022b), "Effects of interface angles on properties of rock-cemented coal gangue-fly ash backfill bi-materials", *Geomech. Geoeng.*, **24**, 81-89. https://doi.org/10.12989/gae.2021.24.1.081.

IC